J|A|C|S COMMUNICATIONS

Published on Web 02/09/2009

Halogen-Induced Corrosion of Platinum

Enrico Doná,[†] Michael Cordin,[†] Clemens Deisl,[†] Erminald Bertel,*[,†] Cesare Franchini,[‡] Rinaldo Zucca,[§] and Josef Redinger[§]

Institute of Physical Chemistry, University of Innsbruck, Innrain 52a, A-6020 Innsbruck, Austria, Computational Materials Physics, University of Vienna, Sensengasse 8, A-1090 Vienna, Austria, and Institute of General Physics, Vienna University of Technology, Getreidemarkt 9/134, A-1060 Vienna, Austria

Received December 11, 2008; E-mail: erminald.bertel@uibk.ac.at

The interaction of halogens with platinum surfaces is an extremely interesting problem in catalysis and semiconductor technology. Halogens serve as platinum mobilizers in both deposition and corrosion or etching processes. $[PtCl_4]^{2-}$ adsorption from an electrolyte and subsequent reduction to metallic Pt clusters is an electrochemical pathway for obtaining highly dispersed, catalytically active Pt surfaces.[1] Halogen-induced etching of platinum surfaces is widely applied in device fabrication, where platinum functions as the electrode metal.[2,3] Cl_2 is routinely used in the etch gas, but its role is not clear.[4,5] Enhancement of etching by addition of CO in the Cl_2 etching plasma was attributed to the formation of volatile species.[6] Here we investigate the halogen−platinum surface interaction in an ultrahigh vacuum (UHV) environment by scanning tunneling microscopy (STM), low-energy electron diffraction (LEED), and density functional theory (DFT) calculations. We show that the dry deposition of Cl_2 in vacuo on the initially clean Pt(110) surface yields an array of Cl and $PtCl_4$ almost identical to that from direct deposition of $[PtCl_4]^{2-}$ onto Au(100) in an aqueous environment, as described by Kolb and co-workers.[1] Furthermore, coadsorption of other less reactive species is observed to promote corrosion by converting adsorbed chlorine into $PtCl_4$. This indicates that the highly ordered $Cl/PtCl_4$/metal system reported here is a universal transition state in both erosion and deposition. In addition, the results provide new insights into the role of promoters of the etching process.

To study the platinum−halogen interaction, we chose the Pt(110) surface. Baking in oxygen, Ar ion sputtering, and finally cycles of low-temperature oxygen adsorption ($T < 140$ K) and flash desorption yielded an extremely clean (1 × 2) missing-row reconstructed surface (Figure 1a). Halogen adsorption was carried out by means of solid-state electrolysis of AgBr or AgCl. The silver halide pellet was kept in a heated glass collimator tube, and the amount of halide molecules produced during electrolysis was calculated from the time-integrated electrolysis current. The sample was positioned in front of the collimator, thereby avoiding contamination and corrosion of the UHV chamber.

First-principles DFT calculations served to determine the Br and Cl bond energies on different adsorption sites and the optimum bonding geometries. The calculations were performed using both the all-electron full-potential linearized augmented plane-wave method (as implemented in the FLAIR package)[7] and the Vienna ab initio simulation package (VASP)[8] within the local density approximation (LDA) and the generalized gradient approximation (GGA). The surface was modeled either by a single slab (FLAIR) or repeated slabs (VASP) up to 11 layers thick. In VASP, the repeated slabs were separated by vacuum layers at least 1 nm thick.

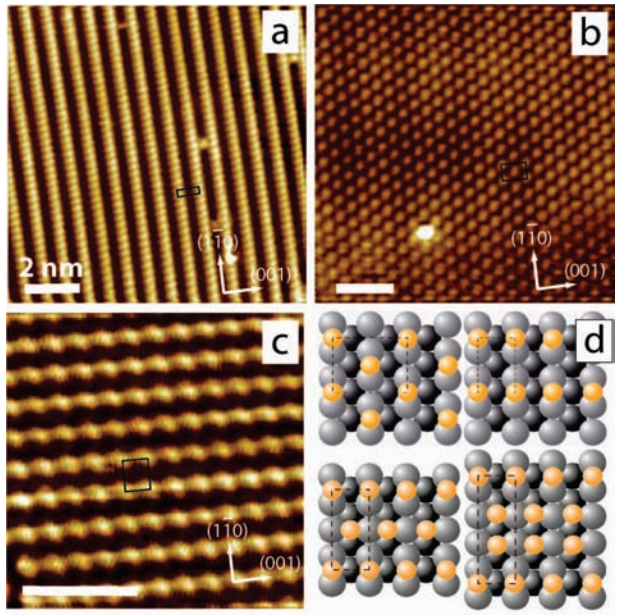

Figure 1. STM images of (a) the missing-row reconstructed Pt(110) surface, (b) the c(2 × 2) Br/Pt(110) adsorbate system, and (c) the (2 × 1) Cl/Pt(110) system. (d) Ball models of the c(2 × 2), (2 × 1), (3 × 1), and (4 × 1) structures. Surface unit cells are shown as rectangles. Grey balls are Pt atoms, and yellow balls are halogen atoms. Scale bars correspond to 2 nm in all images.

The geometry was optimized until all of the forces were less than 0.01 eV/Å. More computational details have been given previously.[9]

Clean Pt(110) exhibits a missing-row reconstruction with a (1 × 2) surface unit cell[10] (Figure 1a). After a dose of 0.5 monolayers [ML; 1 ML is defined by the atom density of the (1 × 1) Pt(110) surface] of Br or Cle atoms is applied, the missing-row reconstruction is lifted and a c(2 × 2) Br/Pt(110) or (2 × 1) Cl/Pt(110) structure, respectively, is formed (Figure 1b,c).[9,11] A halogen coverage (Θ) slightly above 0.5 ML results in a (3 × 1) structure (Figure 1d, bottom left) for both Br and Cl. Further exposure yields a (4 × 1) structure (Figure 1d, bottom right). Both structures were determined by quantitative dynamical LEED (IV-LEED) and ab initio calculations.[12,13] For Br, they are the thermodynamically stable configurations up to the Br desorption temperature, while for Cl they are metastable. Annealing to $T >$ 290 K leads to the appearance of additional four-leaf clover-shaped clusters together with defects in the Cl adlayer. Depending on the precise coverage, domains of the (3 × 1) and (4 × 1) structures are also present, allowing an exact determination of the position of the clusters. Annealing to $T = 670$ K produces a pattern with a fourfold extended unit cell along the [1$\bar{1}$0] direction, i.e., along the close-packed Pt atom rows (Figure 2a). The LEED pattern shows

[†] University of Innsbruck.
[‡] University of Vienna.
[§] Vienna University of Technology.

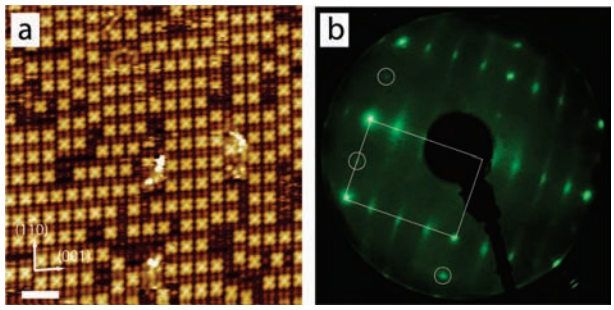

Figure 2. (a) STM image of Cl/Pt(110) with a Cl coverage of ~0.75 ML after annealing to 670 K. The scale bar corresponds to 2 nm. (b) LEED image of the structure shown in (a). The white rectangle denotes the (1 × 1) unit cell of Pt(110). The white circles mark half-order spots indicating a preference for a (4 × 2) ordering.

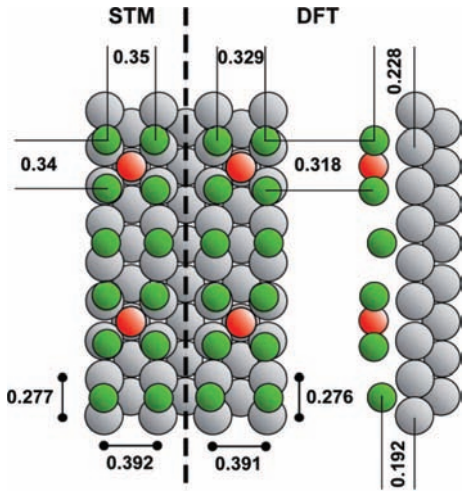

Figure 3. Ball model of the (4 × 2) $PtCl_4$/Cl/Pt(110) adsorbate system. Gray balls are Pt substrate atoms, green balls Cl atoms, and red balls the central Pt atoms of the $PtCl_4$ pentamers. The vertical dashed line separates the experimental STM and calculated DFT (VASP−LDA) results. At the lower left and right, the dimensions of the Pt surface unit cell are given, while at the upper left and right, the distances between the Cl atoms in the $PtCl_4$ clusters are designated. In the side view at the far right, the vertical distances from the Cl atoms and from the $PtCl_4$ clusters to the Pt substrate are given. Almost no buckling (<0.002 nm) is found for either the $PtCl_4$ or the surface Pt layer. A larger buckling (0.02 nm) appears in the second Pt layer. All distances are given in nanometers.

a slight indication of a (4 × 2) periodicity (Figure 2b). However, the periodicity across the rows, i.e., in the [001] direction, is strongly perturbed. The defects in the adlayer disappear upon annealing.

The clover-shaped clusters contain five local corrugation maxima. The central maximum appears to protrude beyond its four satellites when the unoccupied states are sampled by STM (Figure 4a), while in the filled-states image, only the central maximum is seen at all (Figure 4b). Apparently, the local density of states (LDOS) on the central position is significantly higher than on the peripheral ones. If we tentatively associate the maxima with the positions of adatoms, then the position of the central atom is the fourfold hollow position between two close-packed Pt atom rows. In this case, the distance between the peripheral atoms and the central atom in the clover-shaped clusters is ~0.24 nm, while the distance between the peripheral atoms amounts to ~0.35 nm. The remaining Cl atoms between the clover-shaped clusters and the peripheral cluster atoms forming the four "leaves" add up to a coverage of $\Theta = {}^6/_8 = 0.75$ ML, which coincides with our Cl coverage calibration. This and the different LDOS led us to tentatively identify the clover-shaped clusters with $PtCl_4$ units. The fourfold hollow site is in fact the

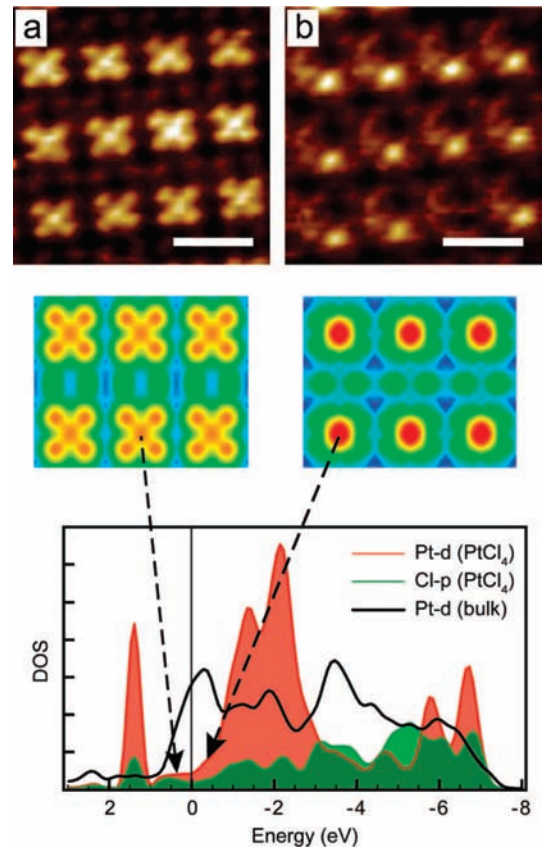

Figure 4. (a) Empty-state STM image of the $PtCl_4$ clusters ($V_{bias} = 0.481$ V; $I_t = 0.342$ nA). (b) Filled-state image of the $PtCl_4$ clusters ($V_{bias} = -0.481$ V; $I_t = 0.343$ nA). Scale bars correspond to 1 nm. The middle panels show the corresponding simulated STM images, and the bottom panel shows the LDOS for the adsorbed $PtCl_4$ unit compared with that for bulk Pt.

naturally favored adsorption site for a Pt adatom. Strong support for this assignment stems from our DFT calculations and the similarity of the observed structure to the results of Kolb and co-workers,[1] as further discussed below.

Although LDA and GGA yield rather similar results in the DFT calculations, LDA was preferred in the present context, as it performs better for the late 5d series.[14] A comparison of the structure inferred from the STM measurements and the optimized geometry obtained from DFT is presented in Figure 3.

The DFT VASP simulations yield a flat $PtCl_4$ structure 0.23 nm above the surface. The Pt−Pt bond distance for the central Pt atom is 0.33 nm, which is a 20% increase with respect to the bulk. This supports the idea of an adsorbed $PtCl_4$ unit as opposed to four chlorine atoms adsorbed around a Pt adatom. The Pt−Cl bond length in K_2PtCl_4 is 0.231 nm,[15] in good agreement with the experimental and theoretical values found here. In addition, we observe a slight distortion of the square-planar configuration. A rigorous test for the adlayer model presented in Figure 3 is provided by a comparison of measured and calculated LDOS, as shown in Figure 4. The agreement is convincing.

As noted above, the formation of $PtCl_4$ units by "excavation" of Pt atoms from the substrate required Cl coverages above 0.5 ML. Remarkably, this corrosion process could also be initiated by adsorbing less reactive species, which compete with Cl for the short-bridge sites. The present findings have several interesting implications: First, we note the formation of a long-range-ordered chain structure containing $PtCl_4$ units alternating with two Cl atoms in the (4 × 2) unit cell. Kolb and co-workers[1] deposited $[PtCl_4]^{2-}$

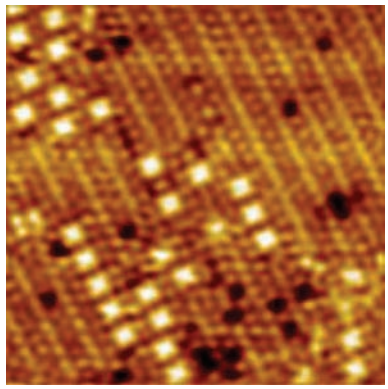

Figure 5. Appearance of four-leaf clover-shaped clusters, indicating the formation of $[PtCl_4]_{ads}$ in a mixed Br/Cl adlayer on Pt(110) prepared at 300 K.

units onto Au(100) and assumed on the basis of their STM images precisely the same alternating-chain structure as found here. Thus, the present data confirm their hypothesis. Furthermore, while the present array self-assembles upon Cl-induced corrosion of the Pt(110) substrate under UHV, the corresponding structure on Au(100) was formed by deposition of $[PtCl_4]^{2-}$ from an electrolyte solution. Consequently, the two opposite processes apparently proceed through the same transition state, with respect to not only the individual species formed, i.e., Cl_{ads} and $[PtCl_4]_{ads}$, but also the same type of long-range order. This is particularly significant in view of the different surface structures and chemistries of the substrates, namely, a (110) surface of a transition metal as opposed to a (100) surface of a noble metal.

As noted above, the activated formation of $PtCl_4$ clusters on Pt(110) requires a (local) coverage above $\Theta_{Cl} = 0.5$ ML. We found, however, that corrosion can also be initiated by exposing the (2×1) Cl/Pt(110) surface to other less reactive species, such as Br_2 (Figure 5) or even CO. Pure Br, in contrast, is not able to attack the Pt substrate, which is also confirmed by DFT calculations: while the energy gain from bonding a Cl atom to the excess Pt atom is comparable to the energy cost of forming a Pt surface defect, an energy deficit of $\sim$1 eV is found for Br. Thus, the effect of coadsorbates with lower corrosion potentials is indirect: they compete with Cl for the short-bridge sites, thereby increasing the chemical potential of Cl in the adlayer. As a consequence, the formation of $[PtCl_4]_{ads}$ becomes thermodynamically favorable. The coadsorbates in the present case thus substitute for raising the potential in $[PtCl_4]^{2-}$ deposition from the electrolyte.

Accordingly, the well-known promotion of chlorine-induced Pt etching by CO may in part be due to the destabilization of a pure Cl adlayer and its transformation into a mixed $Cl-PtCl_4$ adlayer.

Additional support for this scenario is provided by experiments on temperature-programmed desorption of CO from the CO/Br/Pt(110) and CO/Cl/Pt(110) surfaces (Figure 1 in the Supporting Information). A low-temperature desorption peak between 150 and 400 K is qualitatively similar for the two surface systems, allowing a direct comparison of desorbing amounts of CO. Furthermore, in both cases, CO desorption is complete at 550 K. However, in the case of CO−Cl coadsorption, a narrow, autocatalytic desorption peak appears at 425 K, while CO comes off the CO−Br coadsorption layer in a much broader feature at $\sim$480 K. The autocatalytic desorption is driven by the decomposition of the $PtCl_4$ units and the reversal of Cl to its more stable adsorption state in the (2×1) structure. The similarity of the areas under the CO desorption curves for the Cl and Br systems shows that volatile carbonyl species are formed in small traces at most. It should be noted that the autocatalytic desorption feature at 425 K cannot arise from fragmentation of $Pt(CO)_2Cl_2$ because the sublimation temperature of $Pt(CO)_2Cl_2$ is 483 K. The present results therefore do not support formation of $Pt(CO)_2Cl_2$, at least under the mild conditions used here.

In summary, we report the formation of a long-range-ordered mixed $Cl-PtCl_4$ adlayer on Pt(110) upon compression of a (2×1) Cl/Pt(110) layer. The compression can be caused by various atomic and molecular coadsorbates that compete with Cl for the short-bridge adsorption sites. Remarkably, the $Cl-PtCl_4$ adlayer structure is virtually the same on Pt(110) and Au(100). It develops under UHV as well as in an electrolyte and even when only $[PtCl_4]^{2-}$ is deposited, as in the latter case. Codeposition of Cl_2 and CO does not result in the formation of volatile $Pt(CO)_2Cl_2$ species upon heating. While Cl_2 is able to attack the Pt surface to form $PtCl_4$, this is not possible for Br under similar conditions.

Acknowledgment. This work was supported by the Austrian Science Fund through the National Research Network (S9004−N20).

Supporting Information Available: Temperature-programmed desorption spectra of CO coadsorbed with Cl and CO coadsorbed with Br on Pt(110). This material is available free of charge via the Internet at http://pubs.acs.org.

References

(1) Waibel, H.-F.; Kleinert, M.; Kibler, L. A.; Kolb, D. M. *Electrochim. Acta* **2002**, *47*, 1461–1467.
(2) Kim, J. H.; Kim, K. W.; Woo, S. I. *J. Vac. Sci. Technol.* **2004**, *B22*, 1662–1668.
(3) Milkove, K. R.; Coffin, J. A.; Dziobkowski, C. *J. Vac. Sci. Technol.* **1998**, *A16*, 1483–1488.
(4) Shibano, T.; Oomori, T. *J. Vac. Sci. Technol.* **1997**, *B15*, 1747–1751.
(5) Chang, L.-H.; Apen, E.; Kottke, M.; Tracy, M. *J. Vac. Sci. Technol.* **1998**, *A16*, 1489–1496.
(6) Kim, J. H.; Woo, S. I. *Appl. Surf. Sci.* **2000**, *156*, 9–15.
(7) Wimmer, E.; Krakauer, H.; Weimert, M.; Freeman, A. J. *Phys Rev. B* **1981**, *24*, 864–875. Weinert, M., Wimmer, E., Freeman, A. J. *Phys Rev. B* **1982**, *26*, 4571−4578; http://www.uwm.edu/~weinert/flair.html/.
(8) Kresse, G.; Furthmüller, J. *Phys. Rev. B* **1996**, *54*, 11169–11186; http://cms.mpi.univie.ac.at/vasp/.
(9) Blum, V.; Hammer, L.; Heinz, K.; Franchini, C.; Redinger, J.; Swamy, K.; Deisl, C.; Bertel, E. *Phys. Rev. B* **2002**, *65*, 165408.
(10) Hanesch, P.; Bertel, E. *Phys. Rev. Lett.* **1997**, *79*, 1523–1526.
(11) Franchini, C. Ph.D. Thesis, Vienna University of Technology, 2002.
(12) Deisl, C.; Swamy, K.; Memmel, N.; Bertel, E.; Franchini, C.; Schneider, G.; Redinger, J.; Walter, S.; Hammer, L.; Heinz, K. *Phys. Rev. B* **2004**, *69*, 195405.
(13) Deisl, C.; Dona, E.; Penner, S.; Gabl, M.; Bertel, E.; Zucca, R.; Redinger, J. *J. Phys.: Condens. Matter*, in press.
(14) Tran, F.; Laskowski, R.; Blaha, P.; Schwarz, K. *Phys. Rev. B* **2007**, *75*, 115131.
(15) Ohba, S.; Sato, S.; Saito, Y. *Acta Crystallogr.* **1983**, *B39*, 49–53.

JA809674N